Controlling drift-wave turbulence using time-delay and space-shift autosynchronization feedback

Guoning Tang,[1,2] Kaifen He,[3] and Gang Hu[1,4,5,*]
[1]*Department of Physics, Beijing Normal University, Beijing 100875, China*
[2]*College of Physics and Information Technology, Guangxi Normal University, Guilin 541004, China*
[3]*Institute of Low Energy Nuclear Physics, Beijing Normal University, Beijing 100875, China*
[4]*Chinese Center for Advanced Science and Technology (World Laboratory), Beijing 8730, China*
[5]*Beijing-Hong Kong-Singapore Joint Center of Nonlinear and Complex Systems, Beijing Normal University Branch-Beijing, China*
(Received 26 December 2005; revised manuscript received 10 March 2006; published 5 May 2006)

Drift-wave turbulence control in a one-dimensional nonlinear drift-wave equation driven by a sinusoidal wave is considered. We apply time-delay and space-shift feedback signals, to suppress turbulence. By using global and local pinning strategies, we show numerically that the turbulent state can be controlled to periodic states effectively if appropriate time-delay length and space-shift distance are chosen. The physical mechanism of the control scheme is understood based on the energy-minimum principle.

DOI: 10.1103/PhysRevE.73.056303 PACS number(s): 47.27.Rc, 05.45.Gg, 52.35.Kt

I. INTRODUCTION

Spatiotemporal chaos and turbulence occur in a variety of nonlinear dynamical systems. In many practical situations such behaviors are considered to be harmful. For instance, drift-wave turbulence which is caused by pressure-driven instability in magnetized plasmas [1] is generally believed to be responsible for anomalous cross-field particle transport that causes undesirable energy loss [2]. Therefore, spatiotemporal chaos and turbulence control in these systems is of crucial importance. Since spatially extended systems typically contain a very large number of unstable degrees of freedom [3], some dense lattices of controlling nodes are needed for the control purpose and the control of spatiotemporal chaos is more complicated as well as difficult.

Up to the present, many control methods have been suggested to control low-dimensional chaos by stabilizing periodic orbits [4–10]. One of these schemes is time-delay autosynchronization (TDAS) [5], where the control signal is an amplified difference of a suitable observable measured at t and $t-\tau$. Because of its simplicity and robustness, the application of TDAS has attracted much attention of scientists in the past decade [11–24]. Several variants of the original time-delay feedback scheme have been proposed to improve the control performance [24–27], some of which are used to control chaos in spatiotemporal systems [16,28].

Recently, drift-wave chaos and weakly turbulent ionization waves have been experimentally investigated and controlled by using the TDAS techniques [9,29]. However, for spatiotemporal systems TDAS control with large delay time requires a large memory accumulating a large amount of spatiotemporal data for the control purpose. This is inconvenient in practice. In this paper, we propose a method of time-delay and space-shift feedback control to suppress drift-wave turbulence described by a one-dimensional nonlinear drift-wave equation driven by a sinusoidal wave [30,31] with delay time being small or even zero. The main purpose of this paper is to study how to obtain better control performance—i.e., how to reduce the storage data (i.e., by using small delay time) and to decrease the control strength with the number of controllers unchanged.

The paper is organized as follows. In Sec. II, we briefly introduce the driven-damped nonlinear drift-wave equation which is used as our model equation. The control method and the detailed numerical simulation results are given in Sec. III. The physical mechanism underlying this control method is analyzed in Sec. IV. A brief conclusion is presented in the last section.

II. THE MODEL

The model to be studied is a one-dimensional nonlinear drift-wave equation driven by a sinusoidal wave [30–32].

$$\frac{\partial \phi}{\partial t} + a\frac{\partial^3 \phi}{\partial t\, \partial x^2} + c\frac{\partial \phi}{\partial x} + f\phi\frac{\partial \phi}{\partial x} = -\gamma\phi - \epsilon \sin(x-\omega t), \tag{1}$$

where ϕ is a fluctuating electric potential. In the main part of the paper a 2π-periodic boundary condition $\phi(x+2\pi,t)=\phi(x,t)$ is applied. The influences of system size and system boundary condition will be discussed in the end of Sec. IV. Throughout the paper, we fix parameters to $a=-0.2871$, $\gamma=0.1$, $c=1.0$, $f=-6.0$, $\epsilon=0.22$, and $\omega=0.65$, at which the system is deeply in the turbulence regime where the motion is irregular both in time and in space [31,32]. Equation (1) with $\gamma=0$ and $\epsilon=0$ describes nonlinear drift waves in magnetized plasmas, and thus this model is of importance in the field of plasma physics [31,33].

The pseudospectral method with de-aliasing technique [34] is used to simulate Eq. (1). In the numerical simulation, we divide the space of 2π into $I_x=256$ grids. The time increment Δt is chosen to be 10^{-3}. The total integration time length of each run of simulation is 2500. The numerical results are checked and confirmed with refined space and time steps.

In plasma physics, the system energy $E(t)$ is defined as

*Corresponding author. Electronic address: ganghu@bnu.edu.cn

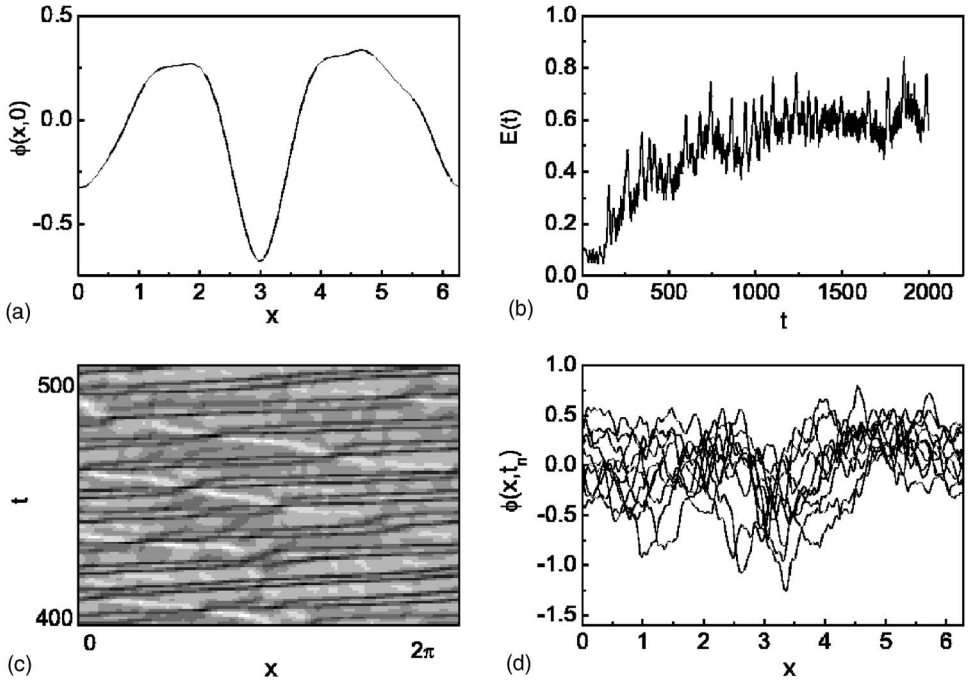

FIG. 1. Dynamic behavior of Eq. (1). (a) Initial electric potential distribution. (b) Evolution of energy $E(t)$ defined in Eq. (2). (c) Space and time distribution of potential $\phi(x,t)$ evolved from the initial condition (a) at $t=0$. (d) Distributions of $\phi(x,t)$ at various moments $t=t_n=nT, T=\frac{2\pi}{\omega}$, and $n\in[249,258]$.

$$E(t)=\frac{1}{2\pi}\int_0^{2\pi}\frac{1}{2}\left[\phi^2(x,t)-a\left(\frac{\partial\phi(x,t)}{\partial x}\right)^2\right]dx. \qquad (2)$$

The initial distribution of ϕ with $E(0)=0.1$ and $\bar{\phi}=\frac{1}{2\pi}f_0^{2\pi}\phi dx=0$ is shown in Fig. 1(a). The time evolution of energy $E(t)$ and the electric potential $\phi(x,t)$ of the system are demonstrated in Figs. 1(b) and 1(c), respectively. In Fig. 1(d), we present $\phi(x,t)$ vs x at various time moments $t=t_n=nT$, where $T=\frac{2\pi}{\omega}\approx 9.666$ and $n\in[249,258]$. It is shown that the state of the system is turbulent [after the system evolves from the initial state of Fig. 1(a) for $t=400$]. In the following we will use this turbulent state as the reference for control.

III. DRIFT-WAVE TURBULENCE CONTROL WITH TIME-DELAY AND SPACE-SHIFT FEEDBACK

The effectiveness of controlling drift-wave turbulence by using chaos control strategies has been verified in the past decade [9,30,31]. In the present work, we suggest a method designed specially for controlling spatiotemporal chaos—that is, time-delay and space-shift injections. With this control we apply additional feedback injections to the right-hand side (RHS) of Eq. (1); then, Eq. (1) is modified to

$$\frac{\partial\phi}{\partial t}+a\frac{\partial^3\phi}{\partial t\,\partial x^2}+c\frac{\partial\phi}{\partial x}+f\phi\frac{\partial\phi}{\partial x}$$
$$=-\gamma\phi-\epsilon\sin(x-\omega t)+\sum_{i=1}^{M}g\,\delta(x-x_i)$$
$$\times[\phi(x+I_s\Delta x,t-\tau)-\phi(x,t)], \qquad (3)$$

where $\Delta x=\frac{2\pi}{I_x}$ is the width of a spatial grid, I_s the number of grid points of space shift, τ the time delay length, M the number of controllers, and g the control strength. We distribute one controller for each J sites, and thus $M=I_x/J$. The control is added to the turbulent state of Fig. 1(c) at $t=500$. For convenience we use a small τ or $\tau=0$.

In order to characterize the control results and qualify the proposed control strategy, we define control error as

$$\sigma(t_n)=\frac{1}{I_x}\sum_{i=1}^{I_x}|\phi(x_i,n_0T)-\phi(x_i,nT)|,$$

$$\sigma=\frac{1}{N}\sum_{n=n_0+1}^{n_0+N}\sigma(t_n). \qquad (4)$$

Here we take $N=10, n_0=248$ (n_0T-500 is the transient time under control). The error σ measures the deviation from periodicity. In the case of a complete control (or, say, exact periodicity), we should have

$$\lim_{t\to\infty}\sigma=0, \qquad (5)$$

and the system reaches a periodic state of period $\frac{2\pi}{\omega}$.

Now we study systematically the effectiveness of the control method of Eq. (3). We first apply global feedback control (i.e., $M=I_x=256$), by fixing $g=0.6$, and studying the control error for different delay times τ and space shifts I_s. In Figs. 2(a) and 2(b), we plot the control error σ vs $\tau[I_s]$ for $I_s=0[\tau=0]$. It is observed that the drift-wave turbulence can be suppressed successfully by either time-delay feedback or space-shift feedback with sufficiently large control strength g

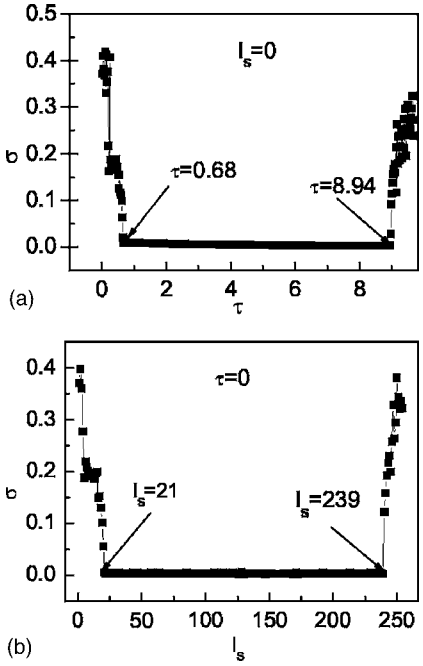

FIG. 2. Asymptotic behavior of control error σ defined in Eq. (4). Global feedback control of Eq. (3) ($M=256, I=J$) is applied. $g=0.6$. (a) σ vs τ with $I_s=0$. (b) σ vs I_s with $\tau=0$.

and suitable delay time τ or space-shift distance I_s. For example, in Fig. 2, when $g=0.6$ one can suppress the turbulence with vanishing space shift if τ is in the range of (0.68, 8.94) or with vanishing time delay if I_s is in the range of (21,239). Though the targets finally reached by different τ's and I_s's are different, all target states are practically periodic with the same period $T=\frac{2\pi}{\omega}$, justified by almost zero control error σ. The obvious advantage for this space-shift feedback over the time-delay feedback is that the former needs much smaller storage of data than the latter.

In order to show the control effect in more systematical manner, we test different combinations of nonzero I_s and τ. In Fig. 3 we plot control error σ vs τ (I_s) for different finite I_s's (τ's). It is observed that with the appropriate choice of I_s and τ the control method in Eq. (3) can suppress the drift-wave turbulence more effectively.

Now we further investigate how to improve the performance of time-delay feedback control with simultaneous space-shift technique. Namely, we focus on how to decrease control strength (i.e., control energy input) for successfully suppressing turbulence by applying optimal matches of I_s and τ. It has been generally accepted that large time delay needs large information process cost and leads to difficulty of successful realization of time-delay feedback control. In this regards, we fix $\tau=0.72$ (relatively small time delay length) and study control error σ for different I_s's by changing the control strength g in a large range, and present the control results in Fig. 4. In Figs. 4(a)–4(c), we applied global control of $M=256(J=1)$. It is observed that purely time-delay feedback control ($I_s=0$) needs a large-g threshold for effective turbulence control and the critical control strength g_c in Eq. (3) can be considerably reduced (nine time smaller) when the time-delay control is associated with some proper choice of I_s (e.g., $I_s=180$). In Figs. 4(d)–4(f) we do the same as Figs. 4(a)–4(c), respectively, by applying local control with much less controllers $M=16(J=16)$. Though this local control becomes much more difficult than the global one, we find still that the drift-wave turbulence can be successfully suppressed by the time-delay and space-shift feedback control under some I_s, and again with an optimal space shift I_s (i.e., $I_s=180$) the time-delay control can suppress turbulence for rather low value of $g(g_c\approx 0.85)$. In the same time the control shows much lower efficiency and even cannot suppress turbulence at all for other space-shift distances with the same density of controllers [e.g., $I_s=0$ in Fig. 4(d) and $I_s=226$ in Fig. 4(f)].

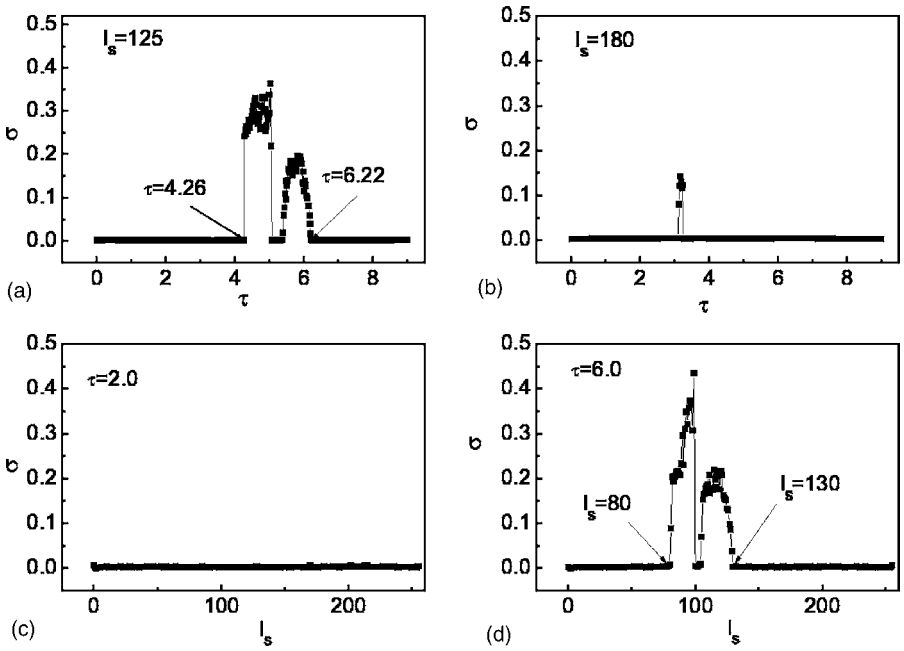

FIG. 3. (a),(b) The same as Fig. 2(a) with nonzero I_s's taken. (c),(d) The same as Fig. 2(b) with nonzero τ's taken.

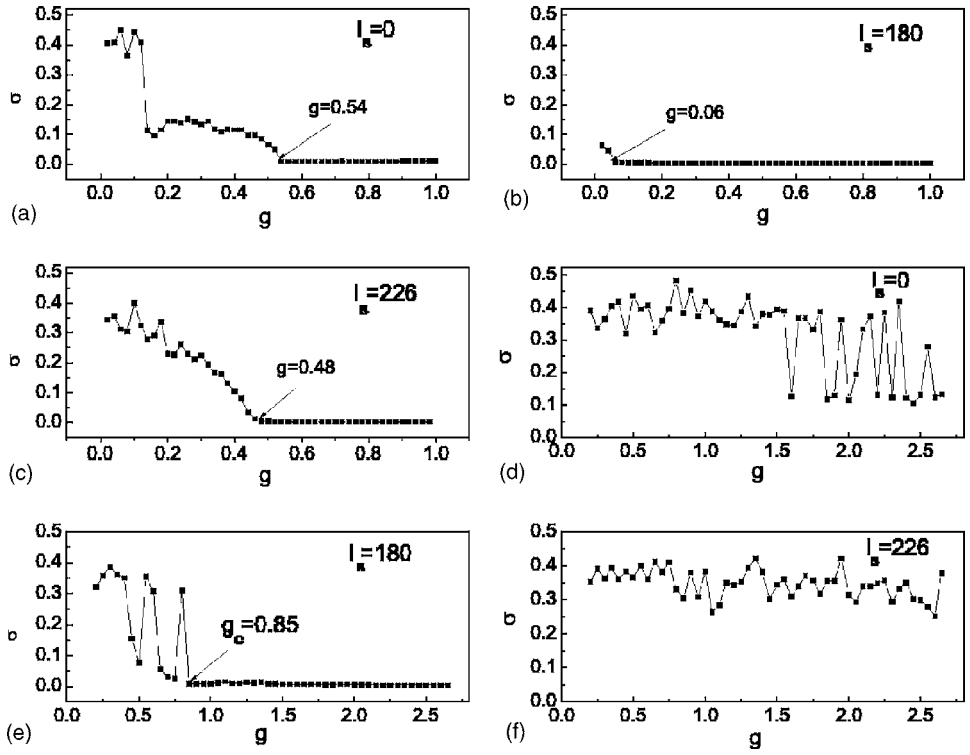

FIG. 4. (a),(b),(c) σ vs g for different I_s's at $\tau=0.72$. The global control strategy of Eq. (3) ($M=256, J=1$) is applied. (d),(e),(f) The same as (a),(b),(c) with local control of $M=16, J=16$ applied.

For having an intuitive impression how changing the space shift distance can change the control results, we plot, in Fig. 5, the asymptotic states of global time-delay and space-shift control for different space shift distances. It is observed that for different I_s's the drift-wave turbulence in Fig. 1(d) can be suppressed. Though the final states under control of different I_s's have quite different shapes of ϕ distributions, the spatial coherence is recovered and the periodicity with period $\frac{2\pi}{\omega}$ has been realized for all these I_s's.

In Fig. 6 we plot g_c, which is the minimum strength for successful control, vs I_s for global feedback control of different τ's. It is found interestingly that in each case there exists some optimal space-shift distance at which g_c takes minimum values over I_s and other I_s's need larger g_c for successful control.

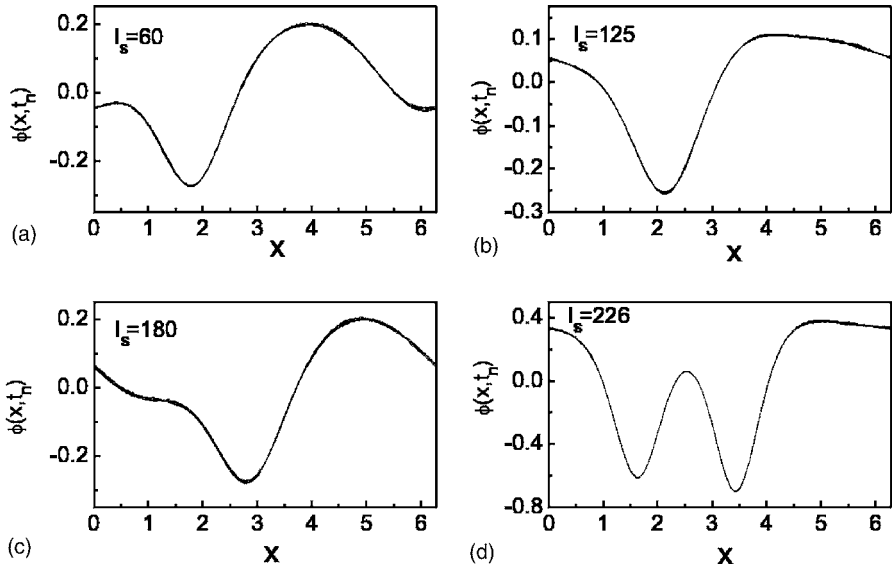

FIG. 5. The same as Fig. 1(d) with dynamics governed by the driven-wave Equation (3) under time-delay and space-shift feedback control. $g=0.6, \tau=0.72$, and I_s's are indicated in the figure frames. Under successful turbulence control with different I_s's all system states become periodic with period $\frac{2\pi}{\omega}$ while the ϕ distributions for different I_s's are quite different.

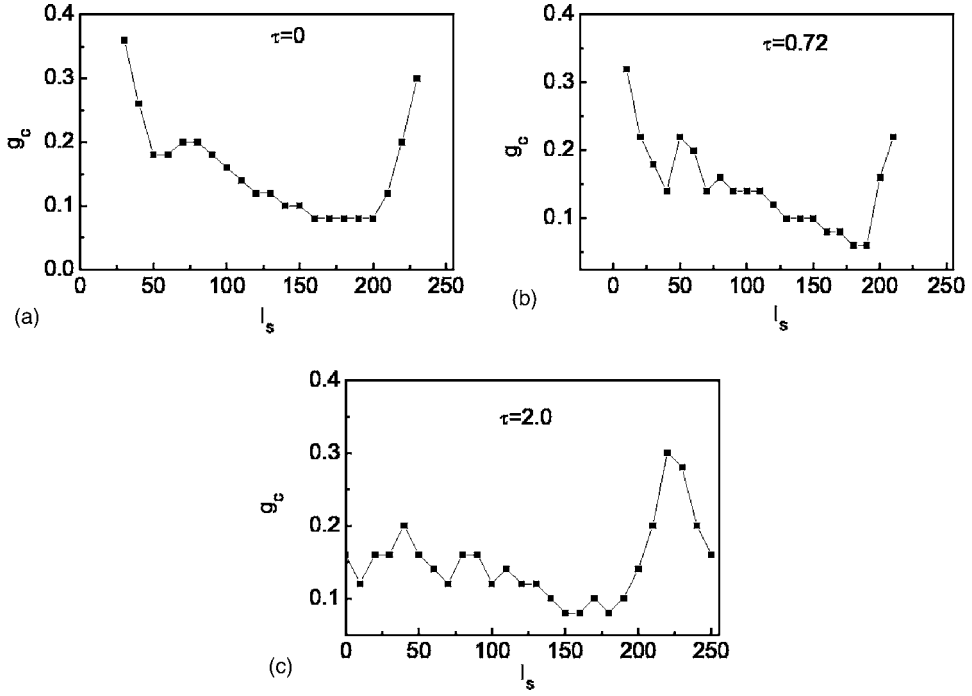

FIG. 6. Critical control strength g_c vs I_s for different τ's. The global control strategy of Eq. (3) ($M=256, I=J$) is applied.

IV. MECHANISM OF OPTIMAL TIME-DELAY AND SPACE-SHIFT FEEDBACK AND THE MINIMUM-ENERGY PRINCIPLE

The above control results can be heuristically understood based on the minimum-energy principle. First, we discuss some theoretical aspects of the controlled driven-wave system (3). By spatially averaging Eq. (3) we obtain

$$\frac{\partial\bar{\phi}}{\partial t}+a\frac{\partial^3\bar{\phi}}{\partial t\,\partial x^2}+c\overline{\frac{\partial\phi}{\partial x}}+f\overline{\phi\frac{\partial\phi}{\partial x}}=-\gamma\bar{\phi}+g[\overline{\phi(x+I_s\Delta x,t-\tau)}-\overline{\phi(x,t)}], \tag{6}$$

where $\bar{\phi}=\frac{1}{2\pi}\int_0^{2\pi}\phi dx$. Under the periodic boundary condition $\phi(x,t)=\phi(x+2\pi,t)$, we have

$$\overline{\frac{\partial\phi}{\partial x}}=\frac{1}{2\pi}\int_0^{2\pi}\frac{\partial\phi}{\partial x}dx=\frac{1}{2\pi}\phi|_0^{2\pi}=0,$$

$$\overline{\phi^j\frac{\partial\phi}{\partial x}}=0,\quad j=1,2,\ldots. \tag{7}$$

Moreover, if the initial distribution of ϕ is set to $\bar{\phi}=0$ (as we do throughout the paper), the solution of Eq. (6) always maintains $\bar{\phi}=0$. Second, let us calculate the system energy $E(t)$ defined in Eq. (2):

$$\frac{dE(t)}{dt}=-c\overline{\phi\frac{\partial\phi}{\partial x}}-f\overline{\phi^2\frac{\partial\phi}{\partial x}}-\epsilon\overline{\phi\sin(x-\omega t)}-\gamma\overline{\phi^2}-g[\overline{\phi^2}-\overline{\phi\phi(x+I_s\Delta x,t-\tau)}]=-\epsilon\overline{\phi\sin(x-\omega t)}-\gamma\overline{\phi^2}-g[\overline{\phi^2}-\overline{\phi\phi(x+I_s\Delta x,t-\tau)}]. \tag{8}$$

By inserting the Fourier transformation of ϕ,

$$\phi(x,t)=A_0+\sum_{m=1}^{\infty}A_m(t)\cos[mx-\beta_m(t)],$$

$$\phi(x+I_s\Delta x,t-\tau)=A_0+\sum_{m=1}^{\infty}A_m(t-\tau)\cos[mx-\beta_m(t-\tau)+mI_s\Delta x], \tag{9}$$

into Eq. (8) and considering $A_0=0$ we have

$$\frac{dE(t)}{dt}=\frac{1}{2}\epsilon A_1(t)\sin[\delta\beta_1(t)]-\gamma\overline{\phi^2}-F(t), \tag{10a}$$

$$F(t)=g\overline{\phi^2}-g\frac{1}{2}\sum_{m=1}^{\infty}A_m(t)A_m(t-\tau)\cos[\Delta\beta_m(t)], \tag{10b}$$

$$\Delta\beta_m(t)=\beta_m(t)-\beta_m(t-\tau)+mI_s\Delta x, \tag{10c}$$

$$\delta\beta_1(t)=\omega t-\beta_1(t), \tag{10d}$$

$$\overline{\phi^2}=\frac{1}{2}\sum_{m=1}^{\infty}A_m^2(t). \tag{10e}$$

From Eq. (10) one observes that the first term in the RHS of Eq. (10a) (named as internal driving) depends on A_1 and the other terms (named as internal damping) depend on A_m^2. When $g=0$ (i.e., without control), the system has small internal damping (small γ) and the first term drives the system to the turbulent states for sufficiently large ϵ. In this case, A_m and β_m vary chaotically in a large range [see Figs. 7(a) and

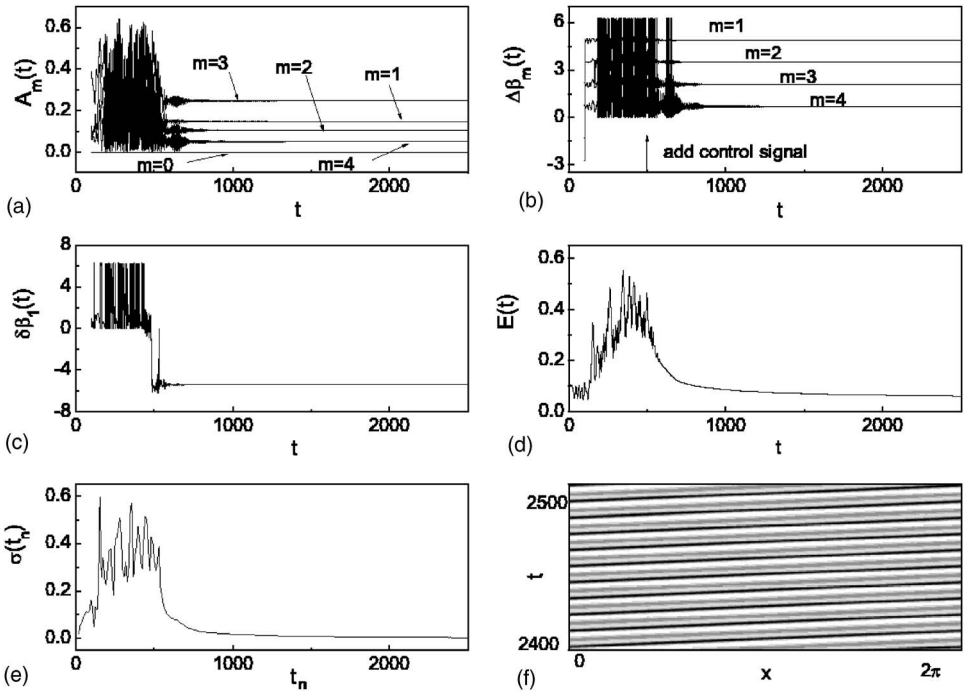

FIG. 7. Characteristic features of global feedback control with $g=0.1, I_s=180$, and $\tau=0.72$. (a) The mode amplitude $A_m(t)$ vs t for different m's. (b) The mode phase difference $\Delta\beta_m(t)$ defined in Eq. (10c) vs t for different m's. (c) $\delta\beta_1(t)$ defined in Eq. (10d) vs t. (d) The energy $E(t)$ vs t. (e) The control error $\sigma(t_n)$ defined in Eq. (4) vs t_n. (f) Spatiotemporal pattern of $\phi(x,t)$ under control after the transient process. The operations of modulo 2π are applied for all mode phase differences. Under successful turbulence control, we observe that for $t \gg 1$: all $A_m(t), \Delta\beta_m(t)$, and $\delta\beta_1(t)$ tend to constants, whose values depend on (τ, I_s). At the same time, $E(t)$ tends to a constant too and $\sigma(t_n)$ vanishes.

7(b) for $t<500$]. When $g>0$ (in Fig. 7 we apply feedback control at $t=500$), there appears an additional damping term $F(t)$ proportional to the feedback control strength g. Moreover, with a suitable choice of τ and I_s the time average of $\cos[\Delta\beta_m(t)]$ may be small and even negative [see Fig. 7(b)].The RHS of Eq. (10a) can be thus made negative definitely if g is sufficiently large and τ and I_s are properly chosen. The energy decreases monotonously under the control until it reaches a minimum constant as the stable periodic target is reached.

In Fig. 7 a number of characteristic features can be clearly seen under successful control. First, all A_m's approach constant values for $t \gg 1$—i.e., $A_m(t) \approx A_m(t-\tau) \approx A_m$ [Fig. 7(a)]. Second, all phase differences $\Delta\beta_m$'s defined in Eq. (10c) approach constant values $\Delta\beta_m$ too for $t \gg 1$, and thus we have $\Delta\beta_m(t) \approx \Delta\beta_m$ [Fig. 7(b)]. Third, $\beta_1(t) \propto \omega t$ [Fig. 7(c)]. Now $F(t)$ can be simplified, for $t \gg 1$, to

$$F = \frac{g}{2}\sum_{m=1}^{\infty} A_m^2(t \to \infty)[1 - \cos(\Delta\beta_m)]. \tag{11}$$

From Eqs. (10a) and (11) the controllability condition reads

$$\frac{g+\gamma}{2}\sum_{m=1}^{\infty} A_m^2 \geqslant \frac{1}{2}\epsilon A_1 \sin(\delta\beta_1) + \frac{g}{2}\sum_{m=1}^{\infty} A_m^2 \cos(\Delta\beta_m), \tag{12}$$

where the equaltiy is valid for complete control at $t \to \infty$, while the inequality is valid in the approach to the periodic target. The concrete values of A_m and the corresponding phase difference of $\Delta\beta_m$ [Eq. (10c)] depend on the distribution shapes of Fig. 5 and thus cannot be computed analytically. However, some definite conclusions can be drawn from the analytical forms of Eqs. (10a) and (12). First, the quantity $F(t)$ is positive definite and $F(t)$ makes the RHS of Eq. (10a) negative definite for sufficiently large g and small $\cos(\Delta\beta_m)$. Consequently, $E(t)$ decreases monotonously to its minimum value when the system reaches its asymptotic state. Moreover, the choice of the optimal combination of τ and I_s can decrease the values of $\cos(\Delta\beta_m)$ of the modes m's with large A_m's and therefore it effectively reduces the control strength threshold g_c. Roughly speaking, the so-called optimal combination of τ and I_s is justified by the optimal phase differences of $\Delta\beta_m$, corresponding to maximum F at a fixed g.

So far our analysis has focused on systems of size 2π with periodic boundary condition. It is emphasized that the method is valid without these restrictions. Since we apply the pseudospectral method for simulations, the space periodic boundary condition is convenient for numerical computations. We can therefore support our above argument with the same boundary condition indirectly by investigating the influence of system size on the efficiency of turbulence control. As system size increases, the turbulence becomes stronger (more positive Lyapunov exponents exist) and the influence of boundary condition to the system dynamics becomes weaker. In Fig. 8 we increase the system size from 2π to 4π [(a),(b),(c)] and 8π [(d),(e),(f)] and apply space-shift

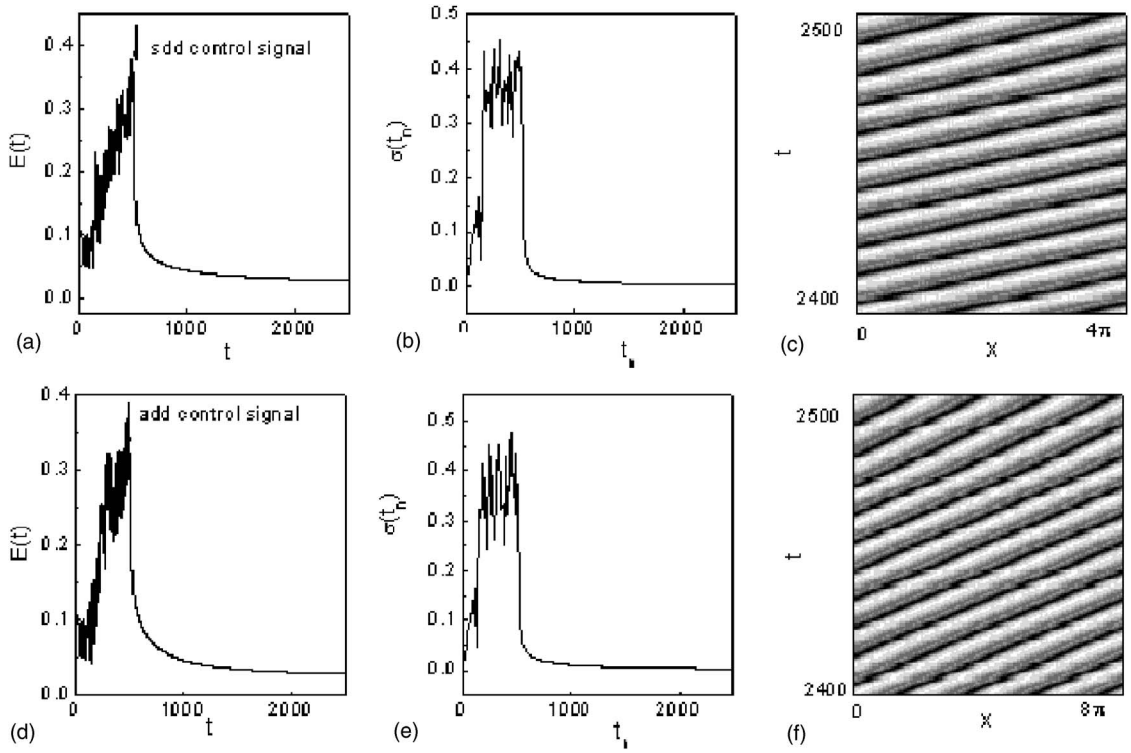

FIG. 8. The results of global control with 4π [(a),(b),(c)] and 8π [(d),(e),(f)] periodic boundary conditions. Time delay $\tau=0$, space shift $I_s=60$, and control strength $g=0.6$ are applied. (a),(d) $E(t)$ vs t_n. (b),(e) $\sigma(t_n)$ vs t. (c),(f) Spatiotemporal ordered patterns of $\phi(x,t)$ after turbulence is suppressed.

control. It is clear that the efficiency of the control approach is not considerably influenced by increasing the system size.

From the demonstration and analysis of Fig. 8 it is obvious that the asymptotic states of successful control under the minimum-energy principle must be stable periodic states of the form $\phi(x,t)=\phi(x-\omega t)$ (otherwise, we cannot reach the minimum energy $\frac{dE}{dt}=0, E=\text{const}$), although the actual forms ϕ's for different τ, I_s, and g can be considerably different.

V. CONCLUSION

In conclusion we have studied the problem of controlling the drift-wave turbulence by time-delay and space-shift feedback control. We find that both space-shift feedback and time-delay feedback can successfully suppress drift-wave turbulence and space-shift operation can considerably improve the time-delay feedback control performance. When the drift-wave turbulence is successfully suppressed, the target state becomes periodic and the energy of the system reaches its minimum value. With the optimal match of time delay and space shift, the control strength threshold can be considerably reduced, and thus the energy of the injected signals for successful control can be greatly reduced too.

For ending this presentation we briefly discuss the type of systems to which the space-shift feedback control applies. From the analysis of Eqs. (10a), (10c), and (12) it seems that space-shift control can be used to suppress turbulence in the system where the time-delay control can tames turbulence to ordered waves periodic in both space and time. The space-shift feedback method may be not applicable in the case that time-delay feedback drives the system to homogeneous oscillating state. On the other hand, the time-delay feedback method may be not applicable too in the case that space-shift feedback drives the turbulent state to a stationary pattern. Therefore, both space-shift and time-delay feedback methods can be applied complementarily in turbulence control. They can also be combinatorially used to optimize control processes.

ACKNOWLEDGMENTS

This work was supported by National 973 project of Nonlinear Science and the Natural Science Foundation of China (Grant Nos. 10335010).

[1] W. Horton, Rev. Mod. Phys. **71**, 735 (1999).
[2] F. Wagner and U. Stroth, Plasma Phys. Controlled Fusion **35**, 1321 (1993).
[3] I. Aranson, H. Levine, and L. Tsimring, Phys. Rev. Lett. **72**, 2561 (1994).
[4] E. Ott, C. Grebogi, and J. A. Yorke, Phys. Rev. Lett. **64**, 1196 (1990).
[5] K. Pyragas, Phys. Lett. A **170**, 421 (1992).
[6] G. Hu and Z. L. Qu, Phys. Rev. Lett. **72**, 68 (1994).
[7] S. Boccaletti, C. Grebogi, Y.-C. Lai, H. Mancini, and D. Maza, Phys. Rep. **329**, 103 (2000).
[8] N. J. Corron, S. D. Pethel, and B. A. Hopper, Phys. Rev. Lett. **84**, 3835 (2000).
[9] T. Klinger, C. Schröder, D. Block, F. Greiner, A. Piel, G. Bonhomme, and V. Naulin, Phys. Plasmas **8**, 1961 (2001).
[10] J. N. Blakely, L. Illing, and D. J. Gauthier, Phys. Rev. Lett. **92**, 193901 (2004).
[11] T. Pierre, G. Bonhomme, and A. Atipo, Phys. Rev. Lett. **76**, 2290 (1996).
[12] C. Simmendinger and O. Hess, Phys. Lett. A **216**, 97 (1996).
[13] W. Just, T. Bernard, M. Ostheimer, E. Reibold, and H. Benner, Phys. Rev. Lett. **78**, 203 (1997).
[14] G. Franceschini, S. Bose, and E. Schöll, Phys. Rev. E **60**, 5426 (1999).
[15] P. Parmananda, R. Madrigal, M. Rivera, L. Nyikos, I. Z. Kiss, and V. Gáspár, Phys. Rev. E **59**, 5266 (1999).
[16] O. Lüthje, S. Wolff, and G. Pfister, Phys. Rev. Lett. **86**, 1745 (2001).
[17] O. Beck, A. Amann, E. Schöll, J. E. S. Socolar, and W. Just, Phys. Rev. E **66**, 016213 (2002).
[18] W. Just, S. Popovich, A. Amann, N. Baba, and E. Schöll, Phys. Rev. E **67**, 026222 (2003).
[19] K. Konishi, Phys. Rev. E **67**, 017201 (2003).
[20] C. Beta, M. Bertram, A. S. Mikhailov, H. H. Rotermund, and G. Ertl, Phys. Rev. E **67**, 046224 (2003).
[21] H. Harrington and J. E. S. Socolar, Phys. Rev. E **69**, 056207 (2004).
[22] A. Ahlborn and U. Parlitz, Phys. Rev. E **72**, 016206 (2005).
[23] A. G. Balanov, N. B. Janson, and E. Schöll, Phys. Rev. E **71**, 016222 (2005).
[24] T. Pyragienè and K. Pyragas, Phys. Rev. E **72**, 026203 (2005).
[25] K. Pyragas, Phys. Lett. A **195**, 206 (1995).
[26] H. Nakajima, Phys. Lett. A **232**, 207 (1997).
[27] K. Pyragas, Phys. Rev. Lett. **86**, 2265 (2001).
[28] M. E. Bleich and J. E. S. Socolar, Phys. Rev. E **54**, R17 (1996).
[29] E. Gravier, X. Caron, G. Bonhomme, and T. Pierre, Phys. Plasmas **6**, 1670 (1999).
[30] H. Guang and H. Kaifen, Phys. Rev. Lett. **71**, 3794 (1993).
[31] H. Kaifen and H. Gang, Phys. Rev. E **53**, 2271 (1996).
[32] Kaifen He, Phys. Rev. Lett. **84**, 3290 (2000).
[33] V. Oraevskii, H. Tasso, and H. Wobig, in *Plasma Physics and Controlled Nuclear Fusion Research*, Proceedings of the Third International Conference, Novosibirsk, 1968 (IAEA, Vienna, 1969), Vol. 1, p. 671.
[34] C. Canuto, M. Y. Hussaini, A. Quarteroni, and T. A. Zang, *Spectral Methods in Fluid Dynamics* (Springer-Verlag, New York, 1987).